Prior-Knowledge-Guided Deep-Learning-Enabled Synthesis for Broadband and Large Phase-Shift Range Metacells in Metalens Antenna

Peiqin Liu, *Member, IEEE*, Liushifeng Chen, and Zhi Ning Chen, *Fellow, IEEE*

***Abstract*—A prior-knowledge-guided deep-learning-enabled (PK-DL) synthesis method is proposed for enhancing the transmission bandwidth and phase-shift range of metacells used for the design of metalens antennas. The algorithm of conditional deep convolutional generative adversarial network is utilized in the proposed deep-learning method. Prior knowledge, including well-known fundamental electromagnetic theorems and experience in antenna design, are purposely applied at the early stage of the proposed method to strategically guide and speed up the synthesis. The proposed intelligent method provides the design of pixelated metacells with high degrees of freedom so that the key performance of the synthesized metacells exceeds the existing limit of conventional design methods by generating a rich profusion of cell patterns. For example, the synthesized triple-layer metacell achieves the –1-dB phase-shift range of 330 ° breaking the limit of 308 ° derived by existing techniques. The proposed synthesis method also provides the additional capability to flexibly control the phase shift not only at the center frequency but also over a frequency range of interest. A Ku-band metalens antenna formed with the synthesized metacells demonstrates the achieved 1-dB and 3-dB gain bandwidths increase by 52.2% and 42.6%, respectively, compared to the metalens antenna using the well-known Jerusalem cross metacells. The proposed method extends the capability for the synthesis of metacells and metalens antennas with enhanced performance.**

***Index Terms*—Deep learning, conditional deep convolutional generative adversarial networks, synthesis method, phase-shift range, gain bandwidth, metacell, metalens antenna.**

I. Introduction

With the development of emerging artificial intelligence (AI)-based technologies, machine-learning (ML) and deep-learning (DL) algorithms attract lots of attention for solving complex problems in electromagnetics [1] , such as remote sensing [2], inverse scattering [3]-[5], microwave device design [6], and antenna design [7]-[9].

Metasurface (MTS) is regarded as a two-dimensional version of metamaterials, which are artificially engineered structure featuring unique electromagnetic properties not found in nature [10]-[12]. MTS provides a great opportunity for the control of electromagnetic waves. It has been intensely used in new low-profile and broadband planar antennas. In applications of MTS-based antennas such as radiators and reflectors, the cell design limits the upper bound of the achievable performance. In particular, the transmission and phase-shift response are essential and challenging. For example, in a transmissive type of MTS lens antennas, the cell with high transmission and wide phase-shift-range over a wide bandwidth are required but cannot be achieved with cells of simple geometry patterns. So far, the study has proven that for metacells with $\lambda/4$ separation between every layer, the existing technical phase-shift limits of –1-dB transmission phase shift for single-, double-, and triple-layer cells are 54 °, 170 °, and 308 °, respectively [13]. The single and double layered cells have reached their physical limits with simple patterns. Furthermore, the cells with triple-layer structures have achieved a phase shift of 308 °, short of the desirable 360 ° full phase shift. Three-layered cells with more complicated patterns have more opportunities to push the phase shift range to the theoretical limit. However, much effort has shown that it is quite challenging to manually craft a set of desired cells due to the design complexity involved.

ML algorithms, including artificial neuronal networks (ANNs) [14], particle swarm optimization (PSO) [15], and genetic algorithm (GA) [16], have been implemented for the optimization and inverse design of MTS antennas [17]-[20]. There are two main categories of antenna geometry optimization. The first involves optimizing the scale of an antenna with a predefined pattern using the ML algorithm [14], [15]. For example, a metacell configured as a triple-layer equal-sized square patch is optimized for the optimal scale, which is the side length of the patch [19]. The metacell retains its original square geometry in the optimization process. The second involves optimizing the geometry pattern of metacells. This is performed by pixelating the planar antenna geometry into a binary matrix with a 1-bit cell status [20]-[23]. By optimizing the binary matrix, the antennas with greater geometrical complexity are generated. The pixelated

This work was partially supported by the Advanced Research and Technology Innovation Centre (ARTIC), the National University of Singapore, under grant R-261-518-002-720.

P. Liu and Z. N. Chen are with the Department of Electrical and Computer Engineering, National University of Singapore, Singapore, 117583 (e-mail: eleczn@nus.edu.sg).

L. Chen is with the Department of Mechanical Engineering, National University of Singapore, Singapore, 117583.

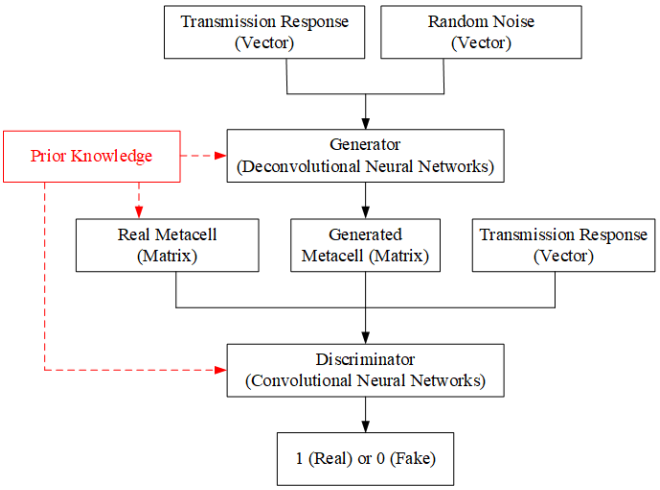

Fig. 1. Schematic diagram of the proposed PK-DL synthesis method.

optimization and design method is also introduced into MTS research [24]-[27]. Although these MTSs are designed with pixelated geometries, their performance has been similarly achieved by conventional design methods.

Prior knowledge should be applied in realizing a prior-knowledge-guided machine-learning-enabled (PK-ML) and deep-learning -enabled (PK-DL) synthesis method for the design of high-performance metacells. In the past years, a deep-learning algorithm, conditional deep convolutional generative adversarial network (cDCGAN), has been presented to generate new graphic patterns in the field of computer vision [28], [29].

In this paper, a PK-DL synthesis method is proposed by introducing the cDCGAN algorithm to generate high-performance metacells with pixelated geometries. On one hand, the synthesis based on the DL algorithms is promising to provide the cell design with the huge potential to break the ceiling of performance in conventional design methods by generating large amounts of novel patterns. On the other hand, training an algorithm from scratch is time consuming with a huge amount of data to be collected. Among the data, only a very small proportion of samples are of interest from a physical aspect. Introducing prior knowledge, including well-known fundamental electromagnetic theorems and experience in antenna design, to guide the algorithm helps to greatly reduce the amount of training data and training time. The triple-layer metacell is utilized as an example to demonstrate the ability of the proposed synthesis method. To verify the design strategy, a metalens antenna is proposed for performance enhancement using the proposed PK-DL synthesis method, benchmarking with a metalens antenna presented using the conventional Jerusalem cross (JC) metacells [30], [31].

II. Conditional Deep Convolutional Generative Adversarial Networks

Fig. 1 shows the schematic diagram of the proposed method. Prior knowledge, including well-known fundamental electromagnetic theorems and experience in antenna design, are applied to guide and speed up the cDCGAN training procedure. Generally, the cDCGAN algorithm is composed of two main components: the generator and the discriminator. The generator is a deconvolutional neural network that learns to generate new content with the same statistical distribution as the training data set. The discriminator is a convolutional neural network (CNN) that learns to distinguish generated content from real content. In the training process, the generator is trained to fool the discriminator and the discriminator is trained to improve its distinguishing ability. These two neural networks compete in the form of a zero-sum game with the goal of producing a generator that is able to generate realistic content.

As shown in Fig. 1, the desired transmission response and random noise (z) are fed into the generator. Then, the generator provides a probability distribution function (PDF) matrix, which represents the pattern of the pixelated metacell. The desired transmission response guides the generator to generate a metacell that has such electromagnetic properties. When it comes to the discriminator, the input data are the transmission response and the geometry matrix of the pixelated metacell. If the geometry matrix of a real metacell is used, the actual transmission response fed into the discriminator is directly obtained from full-wave simulation. Otherwise, if a generated geometry matrix is used, the desired transmission response is fed into the generator. Then, a discriminator CNN is utilized to evaluate the input data of the discriminator. The output of the discriminator is a single scalar in the range of [0, 1]. If the input data is a geometry matrix generated by the generator, the discriminator should output 0. And it should output 1 if the input data is obtained from a real geometry matrix.

The detailed architecture of the cDCGAN algorithm is illustrated in Fig. 2. As shown in Fig. 2(a), the generator network is composed of a deconvolutional neural network with four layers consisting of 256, 128, 64, and N output channels, respectively. The parameter N represents the number of geometry patterns in a multilayer metacell. The input data of the generator network is a combination of two vectors, i.e., desired transmission response and random noise (z), whose dimensions are M and R, respectively. The random noise vector is randomly generated from a uniform distribution. The input data of the discriminator network is a combination of a vector and a geometry matrix. When the geometry matrix is obtained from a real metacell, the vector is sampled from the transmission response of the real metacell. When the geometry matrix is obtained from a generated metacell, the vector is sampled from the desired transmission response.

In the training process, the parameters including M, R, desired frequency range, and the desired transmission responses are tunable. These parameters are selected to ensure that all training data are sampled under the same criteria. Fig. 2(b) shows the architecture of the discriminator network. A real geometry matrix or a generated geometry matrix is fed into a CNN discriminator model that produces a single scalar. The discriminator is composed of five layers with 64, 128, 256, 512, and N output channels, respectively. Every layer in the generator and discriminator networks includes a batch normalization layer and a nonlinear activation function (Leaky ReLu, and Sigmoid) according to the guideline in [28], [29], and [32]. Mathematically, the generator and the discriminator

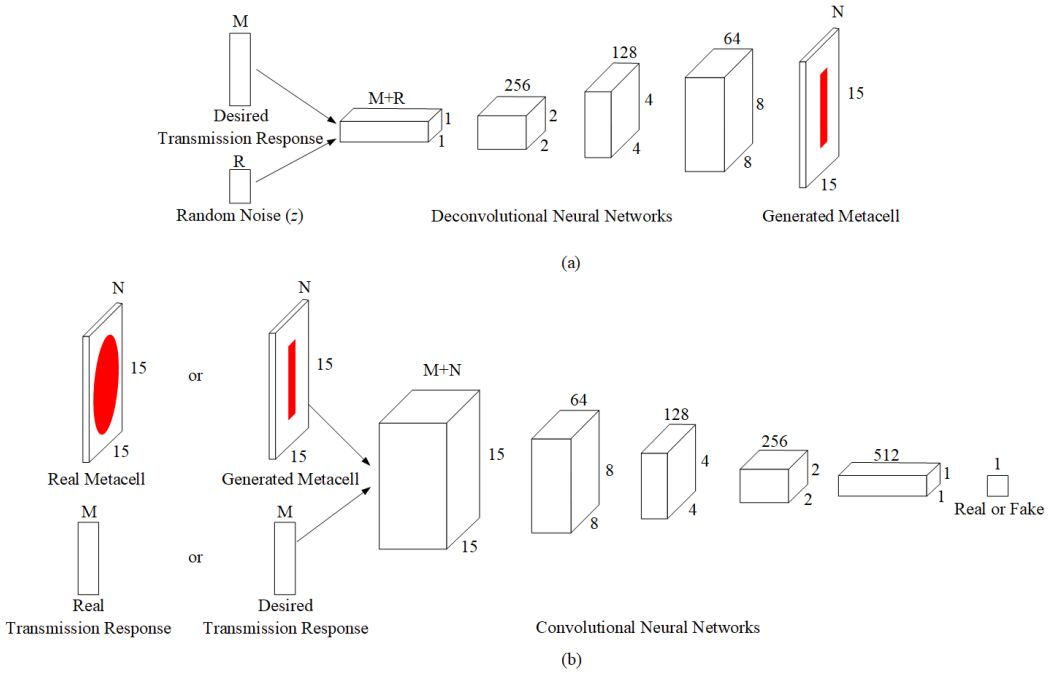

Fig. 2. Architecture of the cDCGAN model. (a) Generator network, and (b) discriminator network.

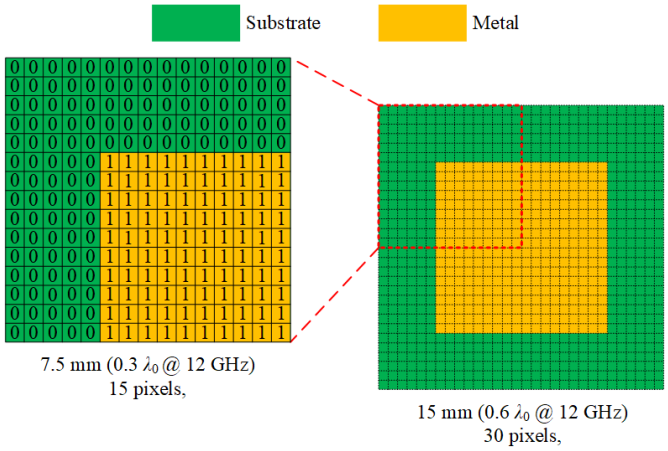

Fig. 3. Schematic diagram of the pixelated metacell.

are optimized in the following two-player minimax game with value function $V(G, D)$ [31]:

$$\min_G \max_D V(D,G) = E_{x\sim p_{data}(x)}[\log D(x)] + E_{z\sim p_z(z)}[\log(1-D(G(z)))] \quad (1)$$

where $D(x)$ evaluates the probability that input x comes from either the real geometry data or the generator, and $G(z)$ represents the output of the generator when it is fed by the desired transmission response and random noise (z). In this proposed method, Adam optimizer is used with learning rate = 2×10^{-4}.

III. DL-Enabled Metacell Design And Analysis

A. Inverse Design of Metacell

Metacells are the unit cells of MTS. The achievable performance of the metacells is the essential constraint of MTS design. The metacells are either single or multiple layered and sized by the periodicity of the MTS, typically around half a wavelength.

Consider a metacell formed by a metallic pattern printed onto a piece of dielectric substrate slab with the dimension around half a wavelength first. Then the metacell is pixelated into binary matrices as shown in Fig. 3. A square metacell with the dimension of 15 mm × 15 mm or 0.6 λ_0 × 0.6 λ_0, where λ_0 is the free-space wavelength at 12 GHz, can be divided into 30 × 30 pixels to form a binary matrix. In this matrix, the value "1" stands for a piece of perfect electrical conductor or metal, and value "0" stands for void (air). In this paper, pixels in the outermost positions of the metacell are set as "0" to form a gap between adjacent unit cells. Thus, this binary matrix provides $2^{28\times28}$ degrees of freedom for the metacell design.

With well-known experience in antenna design, in a metacell with dual-polarization property, the geometry of the metacell keeps mirror symmetrical in horizontal, vertical, and diagonal directions. As a result, only the upper-left quarter of 15 × 15 pixels is utilized as input data in the training process. It should be noted that the geometry in every layer of a multiple layer metacell may be different.

The input data is in a form of tensor with four dimensions, including batch size, height, width, and input channel. Batch size represents the number of the input data used in one iteration of training. Height and width represent the spatial dimensions of the binary matrix. Input channel represents the depth of the input data. If all three layers in a triple-layer metacell, for example, are of the same pattern, the number of input channel is 1. Similarly, if the patterns in all three layers are independent, the number of input channels is 3, one channel for every layer.

When the cDCGAN algorithm is combined with the inverse design of metacells, prior knowledge should be introduced to

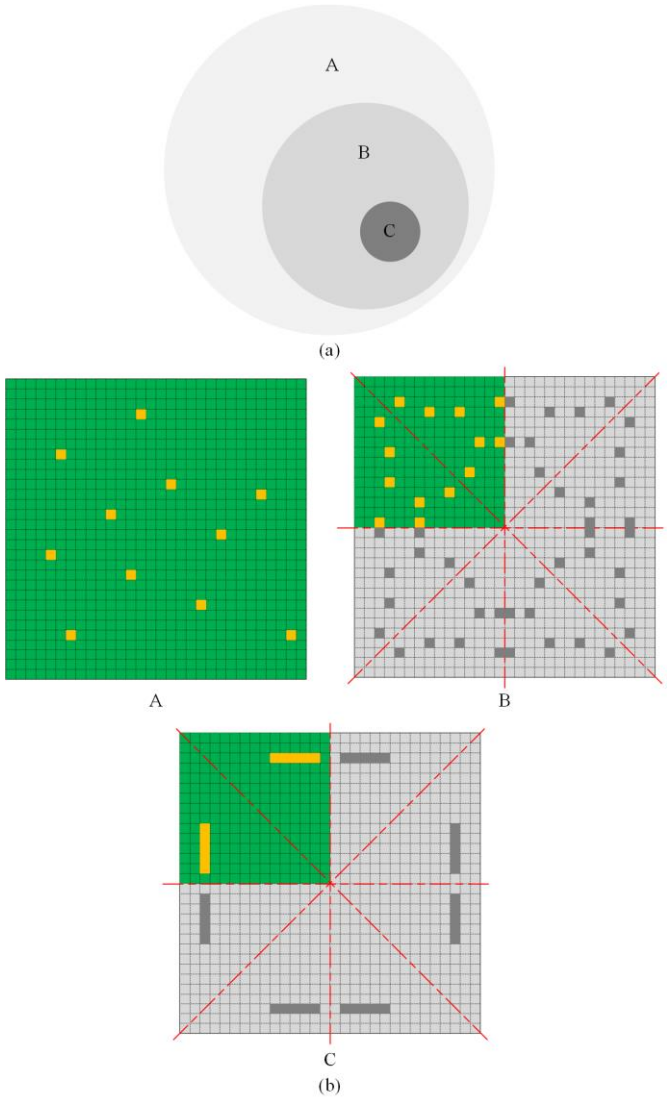

Fig. 4. The methods of generating training data. (a) Relationship between different generating methods. (b) Examples of the generating methods: arbitrary pixels in the whole matrix (Scheme A), arbitrary pixels in the upper-left quarter (Scheme B), and a 1×5-pixel block in the upper-left quarter (Scheme C).

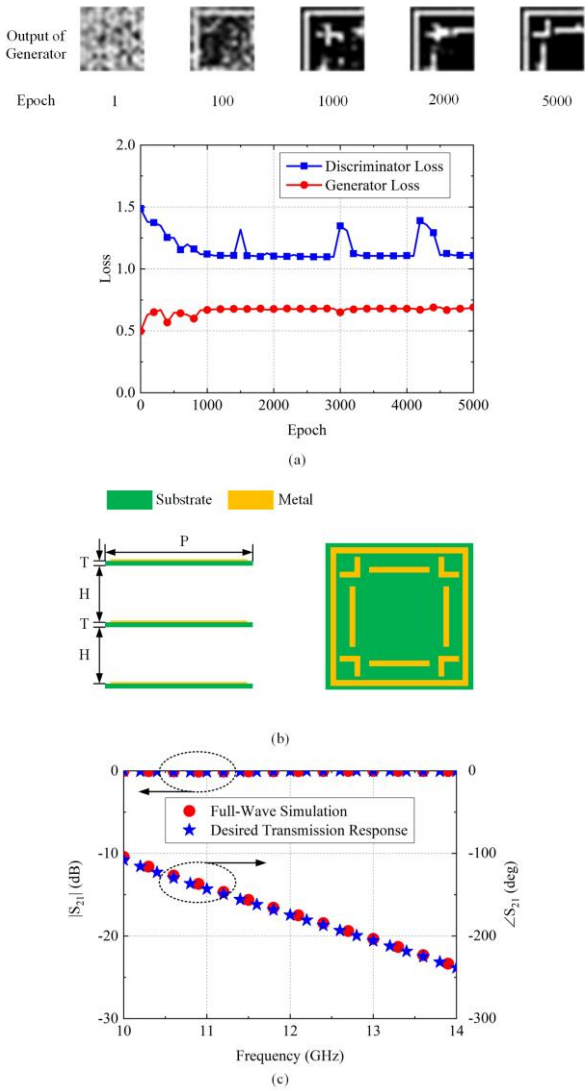

Fig. 5. Effectiveness of the proposed synthesis method. (a) Results of generator and loss during the training process, (b) geometry of the generated triple-layer metacell, and (c) simulated results of the generated metacell. Detailed parameters: P = 15 mm, T = 0.5 mm, H = 5.75 mm.

guide the direction and improve the design efficiency. The prior knowledge includes well-known fundamental electromagnetic theorems and experience in antenna design. First, as abovementioned, the geometry of the metacell is mirror symmetrical in horizontal, vertical, and diagonal directions, which makes the metacell insensitive to polarized incident waves. As a result, the upper-left quarter of the geometry matrix contains all the geometry information. The dimension of the matrix can be reduced from 30 ×30 pixels to 15 ×15 pixels or by 75%.

Second, prior knowledge helps to determine the number of input channels of the input data. In the conventional design method of a triple-layer metacell, all the three layers have identical patterns. The proposed PK-DL synthesis method makes it possible to generate different patterns in every layer of a metacell. This provides much higher degrees of freedom for metacell design. However, according to electromagnetic knowledge, a more efficient way is to keep the patterns on the top and bottom layers of a triple-layer metacell identical. Thus, the structure of the metacell is symmetrical with respect to the middle layer, where patterns on the outer layers mainly contribute to the impedance matching between the metacell and free space.

Third, the prior knowledge from metacell deigns guides the direction for efficiently generating training data. In the proposed method, training data are obtained from the full-wave simulation using electromagnetic simulators.

Schematic diagrams in Fig. 4 show the relationship between three kinds of methods to introduce pixels, namely “0” or “1” into metacells. In the Scheme A as shown in Fig.4, the pixels are arbitrarily introduced into the whole 30 × 30 metacell matrix except the outermost 1-pixel-wide dielectric rim, leading to $2^{28\times28}$ (approximately 1.0×10^{236}) possible patterns. Training model set is too huge to simulate.

In the Scheme B and C, the experience in antenna design suggests that the pattern of metacells in a dual-polarized metalens antenna is mirror symmetrical with respect to

horizontal, vertical, and diagonal directions. Thus, it is sufficient to consider only one-eighth of the metacell matrix so that in the Scheme B, the number of possible patterns is reduced to 2^{105} (approximately 4.06×10^{31}). The exponent 105 is the sum of a finite arithmetic sequence from 1 to 14 with a common difference 1.

Prior knowledge of electromagnetics indicates that the objects with size far smaller than wavelength have less effect on electromagnetic behaviors. Thus, it is not necessary to introduce pixels one by one with a totally random strategy if the size of the pixel is electrically small. As shown in Fig. 3, the size of each pixel is 0.5 mm × 0.5 mm, which is just 0.02 λ_0 × 0.02 λ_0 (λ_0 is the free-space wavelength at 12 GHz). Therefore, a standalone pixel with such a small electrical size has negligible effects on the electromagnetic behaviors. A more efficient way to generate training data is combining several pixels as a basic unit in the order of 0.1 λ_0 and introducing these basic units instead of individual pixels. Thus, a rectangular block with 1 ×5 pixels having an electrical size of 0.1 λ_0 × 0.02 λ_0 is proposed as the new basic unit for introducing pixels into the matrix in the Scheme C. It should be noted that the introduction of the basic unit still follows the mirror symmetrical arrangement. For example, a vertical 1 ×5-pixel block should be introduced accordingly to keep the pattern symmetrical with respect to its diagonal direction when a horizontal 1 ×5-pixel block is introduced. Using the Scheme C, the number of possible models for introducing one basic unit are significantly reduced to only 196. Finally, the training data set can be effectively generated by introducing 1 ×5-pixel blocks into the geometry matrix of metacells.

To train the cDCGAN algorithm, a dataset consisting of more than 6000 metacell models is built up by using ANSYS high-frequency structure simulator (HFSS). These training data are generated using a progressive growth method [42]. The framework of the DL model is based on TensorFlow. Fig. 5 demonstrates the effectiveness of the proposed PK-DL synthesis method.

Fig. 5(a) shows the output images of the generator. The discriminator and generator loss are also presented here. As the number of epochs increases, the discriminator loss and generator loss converge to 1.10 and 0.68, respectively. The final output image is reconstructed into a triple-layer metacell as shown in Fig. 5(b). In this metacell, all the three layers have the same pattern. The periodicity P is $0.6\lambda_0$ = 15 mm. The dielectric substrate is selected as F4B (ε_r = 2.2) in this example. The thickness T of the substrate is 0.5 mm or 0.02 λ_0. The separation H between every layer is 5.75 mm or 0.23 λ_0, which makes the total separation is a quarter wavelength ($H + T$ = 6.25 mm or 0.25 λ_0). Fig. 5(c) shows the desired transmission response and the simulated results of the triple-layer metacell in Fig. 5(b). It is observed that the generated metacell successfully achieves the desired transmission response, which verifies the proposed PK-DL synthesis method for the inverse design of pixelated metacells.

B. Break the Phase-Shift Limit at Center Frequency

In metalens antenna design, the phase-shift range of the metacell is important for the achievable performance of the lens. For a triple-layer metacell with a $\lambda_0/4$ separation between layers, the maximum −1-dB phase-shift range is derived as 308 ° in [13]. The proposed PK-DL synthesis method is expected to break this technical limit and push it closer to the physical limit of 360 °.

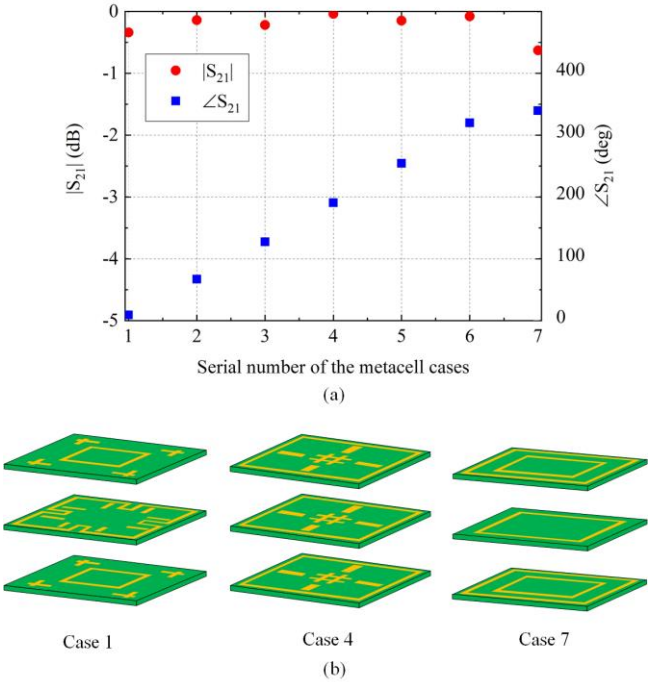

Fig. 6. -1-dB phase-shift range of the proposed synthesis method. (a) Magnitude and phase responses of seven DL synthesized metacells at 12 GHz, and (b) three examples of the DL synthesized metacells.

Fig. 6 shows the transmission response of metacells designed by the proposed method. At the center frequency of 12 GHz, these metacells realize a phase-shift range of 330 ° with the magnitude of transmission coefficient less than −1 dB. It should be noted that even with the help of the proposed synthesis method, it is not easy to break the phase-shift limit. At first, the cDCGAN model is trained using triple-layer metacells that have identical pattern in all three layers. In this configuration, the parameter N in Fig. 2 is 1. Although it could provide a relatively large phase-shift range, the output results cannot break the phase-shift limit of 308 °. Then, the metacells are simulated with full-wave simulation software by using the sandwich configuration, which has two different kinds of patterns in three layers. The cDCGAN model is also re-trained because the parameter N in Fig. 2 should be set as 2. Such an increase in the degree of freedom significantly enhances the complexity of metacell design. It is challenging to design such metacells with a conventional parameter sweeping method.

Finally, Fig 6 shows seven metacell cases which successfully cover the −1-dB phase-shift range from 4.3 ° to 334.5 ° or maximum phase shift of 330 °, breaking the limit of 308 ° for −1-dB transmission. Cases 1, 4 and 7 in Fig. 6 are presented as examples to demonstrate the difference between the pattern configurations of the seven metacells. In Cases 1 and 7, the top and the bottom layers have the same patterns while the middle

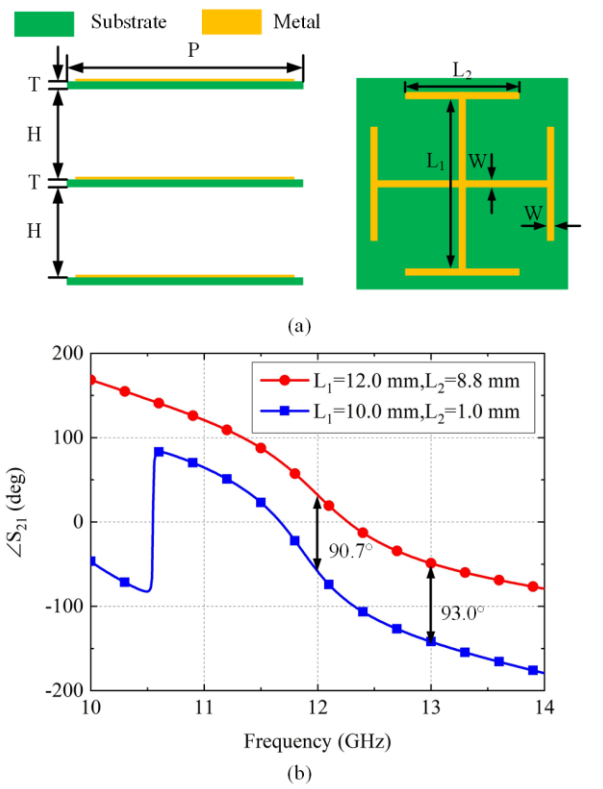

Fig. 7. Phase shift in conventional metacell. (a) Triple-layer unit cell based on Jerusalem cross structure. Detailed parameters: P = 15 mm, T = 0.5 mm, H = 5.75 mm. (b) Transmission phase of Jerusalem cross unit cell with dimension: L_1 = 12 mm, L_2 = 8.8 mm, and L_1 = 10.2 mm, L_2 = 1.0 mm.

layer has a different one. In case 4, all the three layers have the same patterns. It should be noted that the phase-shift limit of 308 ° for −1-dB transmission is derived with approximations [13]. Although the proposed method breaks this approximated limit, it still has a gap to reach the real physical limit of 360°. In conventional methods, metacells are designed with the same geometry pattern in multiple layers due to the design complexity. In the proposed method, there could be varying geometry patterns. The proposed method provides more degrees of freedom for multilayer metacell design and push the upper bound closer to the theoretical limit of triple-layer metacells.

C. Control Phase Shift Over Frequency Range

In metacell design, conventional design methods always focus on transmission responses at the center frequency. However, in a broadband metalens design, phase-shift error would occur off the center frequency, which degrades the gain bandwidth of metalens antennas [34]. The proposed PK-DL synthesis method can provide higher degrees of freedom for flexibly controlling phase shift at off-center frequencies because the patterns or dimensions of metacells have no correlation with any of others. It helps mitigating the phase-shift error and improving the gain bandwidth. To demonstrate the effect of the proposed method, a triple-layer metacell is proposed with the conventional Jerusalem cross (JC) metacell used in [12] and [31] as benchmark.

Fig. 7(a) shows the pattern of the metacell. All three layers

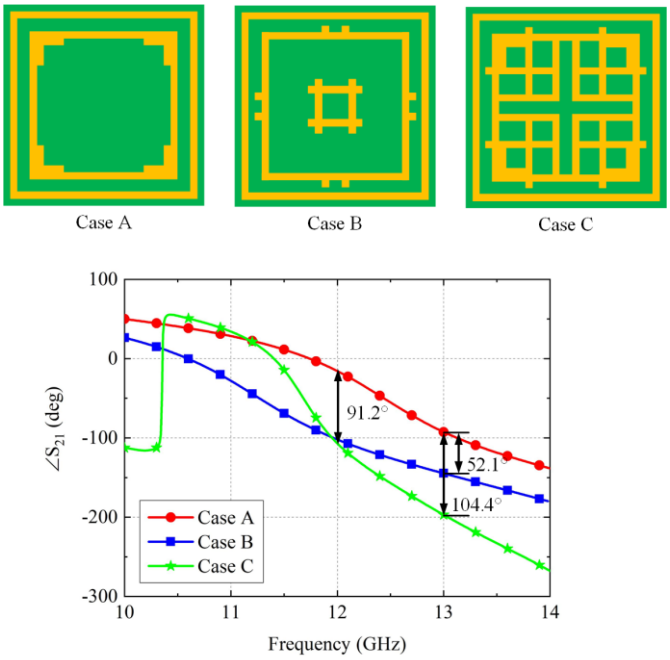

Fig. 8. Transmission phase of metacells using the proposed synthesis method.

have identical JC pattern. The periodicity P, the thickness T of substrate, and the distance H are the same as the metacell in Fig. 5(b). Full-wave simulation shows that at the center frequency the JC metacell can provide a 360 ° phase-shift range with the magnitude of transmission responses less than -3 dB rather than for −1-dB transmission. Suppose that a JC metacell with the dimensions of L_1 = 12.0 mm and L_2 = 8.8 mm is implemented at the aperture center of a metalens antenna and it is set as the reference point of the transmission phase. In another position of the antenna aperture, an element requires 91 °phase-shift delay realizing uniform phase distribution at the center frequency of 12 GHz. According to the full-wave simulation, there is only one choice, i.e., L_1 = 10.0 mm and L_2 = 1.0 mm, that satisfies the phase-shift requirement. Fig. 7(b) depicts the phase responses of these two JC metacells against frequency. The phase-shift delay at 12 GHz is 90.7 °while the phase-shift delay at 13 GHz is 93.0 °. There is no other choice to change the phase shift at 13 GHz because of the phase-shift requirement at the center frequency of 12 GHz. As a result, there is no way in the JC metacell to control the phase shift at off-center frequencies.

By contrast, the PK-DL synthesis method can provide higher degrees of freedom for metacell design. Fig. 8 shows the simulated results of three metacells designed by the proposed method. When Case A is utilized as the phase reference of the metalens antenna, both Cases B and C provide 91 ° phase-shift delay at the center frequency of 12 GHz. At 13 GHz, the phase-shift delay of Cases B and C are 52.1 ° and 104.4 °, respectively. The proposed synthesis method makes it possible to control the phase-shift performance at off-center frequencies when the requirement of phase shift at the center frequency is satisfied. It helps improving the gain bandwidth of the metalens antenna.

To demonstrate the effects of the proposed method on metalens antenna design, two metalens antennas are compared.

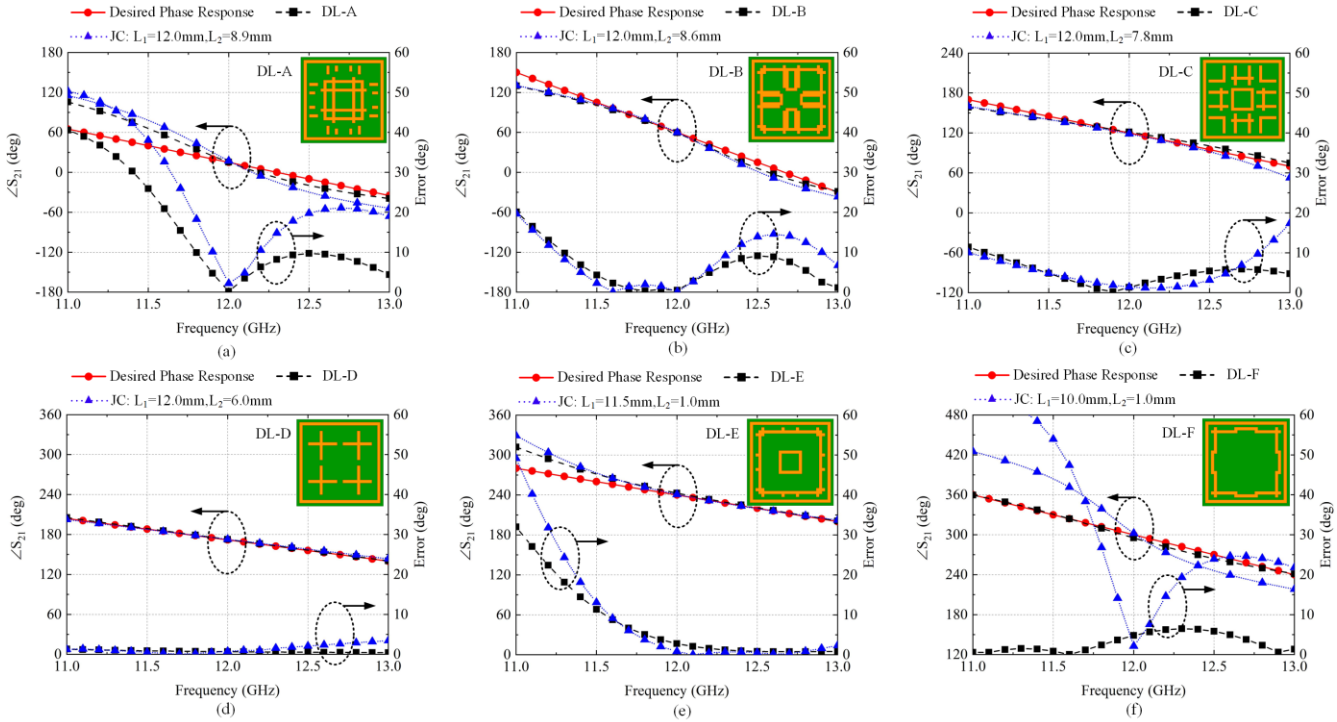

Fig. 9. Comparison between the DL synthesized metacells and JC metacells.

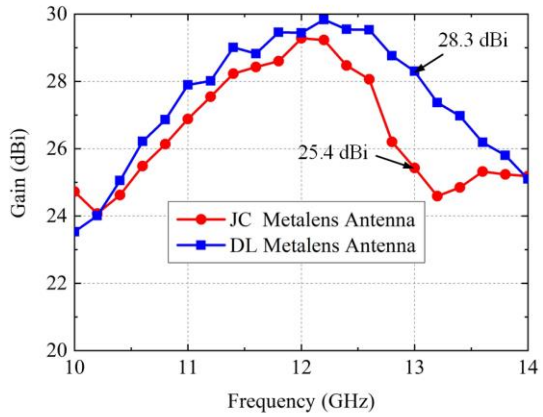

Fig. 10. Gain comparison between metalens antennas designed by using the Jerusalem cross metacell and the proposed deep-learning-enabled metacell.

One metalens antenna is designed using the JC metacell and the other one using the proposed synthesis method. Both the metalens antennas have a square aperture with a side length =330 mm or 13.2 λ_0 at 12 GHz. There are 22 × 22 = 484 triple-layer elements in each metalens antenna. Focal ratio of both metalens antennas is F/D = 0.8. Metacells in the JC metalens antenna are selected for phase compensation only at 12 GHz while the DL-enabled metalens antenna considers the transmission phase at both 12 GHz and 13 GHz.

It should be noted when use the proposed synthesis method to design a metalens antenna, the geometry patterns of adjacent metacells could be very different in terms of patterns. In the proposed metalens antenna, a square metal ring is set as a default structure in every metacell. This makes geometry patterns of these metacells more similar and contributes to stabilizing the mutual coupling between adjacent metacells.

Fig. 9 illustrates phase response comparison between the DL synthesized metacells and JC metacells in these two metalens antennas with six selected samples. At the center frequency of 12 GHz, these metacells realize the phase response of S_{21} around 0 °, 60 °, 120 °, 180 °, 240 °, and 300 °, respectively. The error in Fig. 9 is the difference between the desired phase response and the realized phase response of S_{21} in the DL synthesized metacells and JC metacells. The desired phase response is a straight line, which is determined by the phase response at 12 GHz and 13 GHz. The desired phase response at the center frequency of 12 GHz can be obtained by calculating the phase distribution in the surface of the metalens antenna. The desired phase response at 13 GHz is tunable. In the proposed method, one should tune the desired phase response to make the algorithm coverage.

From Fig. 9, one can observe that compare to JC metacells, the DL-A, DL-B, DL-C, and DL-F metacell in Figs. 9(a), (b), (c), and (f) have smaller phase response errors at the off-center frequency of 13 GHz. The performance of DL-D and DL-E metacell are similar to JC metacells. Although the proposed method mitigates the phase-shift error at off-center frequencies, it cannot completely solve the dispersion problem in metalens antenna design.

Fig. 10 shows the simulated gain of the two metalens antennas. Because both two metalens antennas can realize a uniform phase distribution at the center frequency, the gain of these two metalens antennas is very close at 12 GHz. As the operating frequency increases to 13 GHz, the gain of the JC metalens antenna drops to 25.4 dBi. Owing to the effects of flexibly controlling phase shift at off-center frequencies, the DL-enabled metalens antenna achieves a higher gain of 28.3

Fig. 11. Photograph of the metalens antenna using the proposed synthesis method.

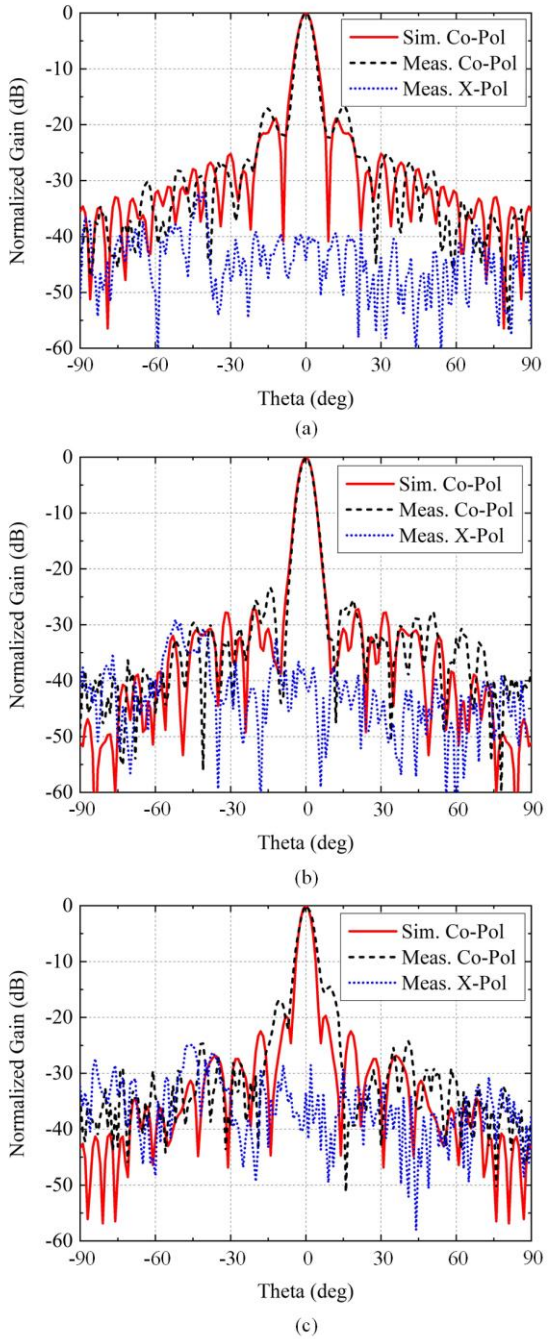

Fig. 12. Simulated and measured results of normalized radiation pattern in the H-plane (xz-plane) at (a) 11 GHz, (b) 12 GHz, and (c) 13 GHz.

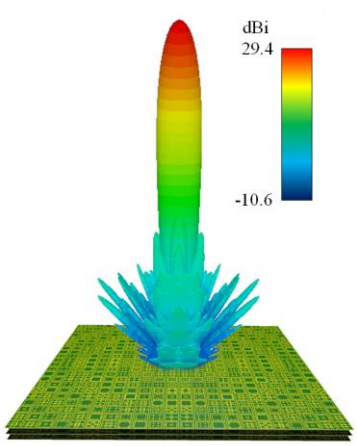

Fig. 13. Simulated 3D radiation pattern of the proposed metalens antenna at 12 GHz.

dBi at 13 GHz. The 1-dB and 3-dB gain bandwidth of the JC metalens antenna are 9.2% and 16.9%, respectively while the DL-enabled metalens antenna realizes the 1-dB and 3-dB gain bandwidth of 14.0% and 24.1% or 52.2% and 42.6% improvement, respectively.

IV. Experimental Results

A prototype of the DL-enabled metalens antenna was fabricated and measured to verify the design strategy. Fig. 11 shows the photograph of the triple-layer metalens antenna. It is formed by three layers of F4B substrate (ε_r = 2.2). A standard gain horn antenna (waveline inc. 699) is positioned at the focal point to illuminate the proposed metalens antenna. At 12 GHz, the gain of the horn antenna is 15.5 dBi and the 3-dB beamwidth is 24 °.

Fig. 12 shows the normalized H-plane (*xz*-plane) radiation patterns at 11 GHz, 12 GHz, and 13 GHz, respectively. The simulated and measured main beams agree well with each other in all these frequencies. Full-wave simulation shows the simulated cross-polarization levels of the proposed metalens antenna are lower than -90 dB. The simulated cross-polarization results are too small so that they are omitted in here for simplicity. In the broadside direction, the measured cross-polarization levels are lower than –35 dB. In the measurement, the separation between the substrate layers of the metalens antenna is not as even as the simulated model. The discrepancies between simulated and measured radiation patterns are due to the assembly error. Because the proposed metalens antenna is dual-polarized and it has a symmetrical configuration, the E-plane radiation patterns of the proposed metalens antenna are similar to the H-plane radiation patterns. Thus, the E-plane patterns are omitted here for simplicity. Fig. 13 illustrates the simulated 3D radiation pattern of the metalens antenna at 12 GHz.

Fig. 14 shows the simulated and measured gain versus frequency. At 12 GHz, the simulated and measured gain of the proposed metalens antenna is 29.4 dBi and 28.4 dBi, respectively. The realized aperture efficiency is 31.6%. The measured results show that 1-dB and 3-dB gain bandwidth of the proposed metalens antenna are 13.5% and 23.9%,

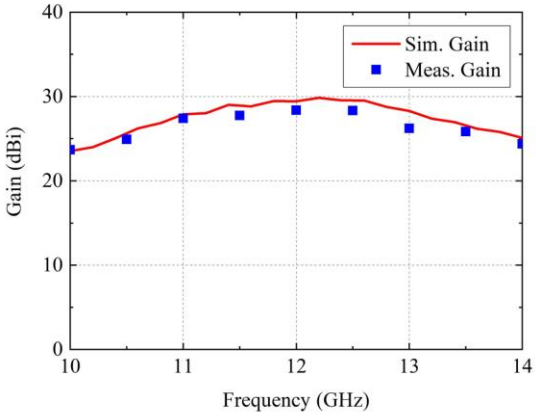

Fig. 14. Simulated and measured gain of the proposed metalens antenna.

TABLE I
COMPARISON OF MEASURED PERFORMANCE

Ref.	Freq. (GHz)	Number of layers	Gain (dBi)	e_{ap} (%)	1-dB gain BW (%)	3-dB gain BW (%)
[33]	30.25	4	28.6	35.6	7.5	N/A
[34]	13.5	4	29.9	47	11.7	N/A
[35]	13.58	4	23.9	55	7.4	N/A
[36]	12.5	3	18.9	20.9	9.6	N/A
[37]	11.3	3	28.9	30	9	19.4
This work	12.0	3	28.4	31.6	13.5	23.9

respectively, wider than those of all the references as compared in Table I. Table I compares the measured performance of the proposed DL-enabled metalens antenna to five previous works. In metalens design, the larger number of layers contributes to progressive impedance matching. Thus, compared to triple-layer metalens antennas, four-layer metalens antennas reported in [33]-[35] achieved higher gain and aperture efficiency at the center frequency. In this work, the proposed method provides an effective way to control phase shift of metacells at off-center frequencies. As a result, the proposed triple-layer metalens antenna realizes the widest 1-dB and 3-dB gain bandwidths among the triple-layer and four-layer metalens antennas in Table I.

Table II compares the designs of the proposed method to other metasurface designs using machine-learning and deep-learning algorithms. Generative adversarial network (GAN) is a popular algorithm in the design of infrared metamaterial [24], [25], [40]. At microwave bands, transfer learning and REACTIVE were utilized to design reflective metamcells. Based on these methods, an abnormal reflection metasurface and a triple-band absorber were realized in [26] and [41], respectively. In this work, cDCGAN, which is another approach of GAN, is introduced into the design of transmissive metacell at the microwave band. A metalens antenna is designed and fabricated to verify the proposed method.

V. CONCLUSION

A PK-DL synthesis method has been proposed for the inverse design of metacells and then applied to a broadband metalens antenna. The cDCGAN algorithm has been introduced to generate pixelated metacells. Prior knowledge, including well-known fundamental electromagnetic theorems and experience in antenna design, has been purposely applied to guide the direction of the algorithm and the metacell design. Compared with conventional design methods, the PK-DL synthesis method has broken the limits in conventional design methods and generated high-performance metacells. The study has shown that these metacells have broken the phase-shift limit at the center frequency and flexibly controlled the phase shift over a wider frequency range. For a triple-layer metacell with $\lambda_0/4$ separation between layers, the phase-shift limit for –1-dB transmission has been improved from 308 ° to 330 °. The Huygens' MTS realizing 360 ° phase shift with double-layer structure was reported [38], [39]. These metacells have a very close distance, instead of $\lambda/4$ separation, between each layer. Moreover, the proposed synthesis method has generated broadband triple-layer metacells to flexibly control the phase shift at off-center frequencies. It has improved gain bandwidth of metalens antennas.

TABLE II
COMPARISON OF METASURFACE DESIGN BASED ON ML

Ref.	Freq.	Algorithm	Metacell Type	Metasurface Type
[24]	400 THz	GAN	Transmissive	N/A
[40]	300 THz	GAN	Reflective	N/A
[25]	70 THz	GAN	Reflective	N/A
[26]	10 GHz	Transfer learning	Reflective	Reflection metasurface
[41]	10 GHz	REACTIVE	Reflective	Absorber metasurface
This work	12 GHz	GAN	Transmissive	Metalens

A Ku-band metalens antenna prototype has been fabricated to verify the proposed method for applications, such as satellite communication. The measured results have shown that 1-dB and 3-dB gain bandwidth of the proposed metalens antenna have reached up to 13.5% and 23.9%, respectively. Compared to a conventional metalens antenna using the JC metacells, 1-dB and 3-dB gain bandwidth have been increased by 52.2% and 42.6%, respectively. Therefore, the proposed PK-DL synthesis method can provide a promising way for designing pixelated metacells and metalens antennas with outstanding electromagnetic performance.

This work has focused on the geometry design of metacells. In the future, more parameters, such as periodicity, separation, substrate thickness, and permittivity, can be taken into consideration to enhance design freedom. The PK-DL synthesis method could be utilized to further push the phase shift limit of metacells to the performance ceiling of the Huygens' MTS. The performance enhanced metacells will be applied to more device design.

REFERENCES

[1] A. Massa, D. Marcantonio, X. Chen, M. Li, and M. Salucci, "DNNs as applied to electromagnetics, antennas, and propagation—a review," *IEEE Antennas Wireless. Propag. Lett.*, vol. 18, no. 11, pp. 2225–2229, Nov. 2019.

[2] S. Chen, H. Wang, F. Xu, and Y.-Q. Jin, "Target classification using the deep convolutional networks for SAR images," *IEEE Trans. Geosci. Remote Sens.*, vol. 54, no. 8, pp. 4806-4817, Aug. 2016.

[3] Y. Zhou, Y. Zhong, Z. Wei, T. Yin, and X. Chen, "An improved deep learning scheme for solving 2-D and 3-D inverse scattering problems," *IEEE Trans. Antennas Propag.*, vol. 69, no. 5, pp. 2853–2863, May. 2021.

[4] Z. Ma, K. Xu, R. Song, C.-F. Wang, and X. Chen, "Learning-based fast electromagnetic scattering solver through generative adversarial network," *IEEE Trans. Antennas Propag.*, vol. 69, no. 4, pp. 2194–2208, Apr. 2021.

[5] R. Guo, Z. Jia, X. Song, M. Li, F. Yang, S. Xu, and A. Abubakar, "Pixel- and Model-based microwave inversion with supervised descent method for dielectric targets," *IEEE Trans. Antennas Propag.*, vol. 68, no. 12, pp. 8114–8126, Dec. 2020.

[6] F. Wang, V. K. Devabhaktuni, and Q.-J. Zhang, "A hierarchical neural network approach to the development of a library of neural models for microwave design," *IEEE Trans. Microwave Theory Tech.*, vol. 46, no. 12, pp. 2391–2403, Dec. 1998.

[7] H. J. Delgado, M. H. Thursby, and F. M. Ham, "A novel neural network for the synthesis of antennas and microwave devices," *IEEE Trans. Neural Netw.*, vol. 16, no. 6, pp. 1590–1600, Nov. 2005.

[8] P. M. Watson and K. C. Gupta, "EM-ANN models for microstrip vias and interconnects in dataset circuits," *IEEE Trans. Microwave Theory Tech.*, vol. 44, no. 12, pp. 2495–2503, Dec. 1996.

[9] Q. Wu, H. Wang, and W. Hong, "Multi-stage collaborative machine learning and its applications to antenna modeling and optimization," *IEEE Trans. Antennas Propag.*, vol. 68, no. 5, pp. 3397–3409, May. 2020.

[10] T. Li and Z. N. Chen, "Compact wideband wide-angle polarization-free metasurface lens antenna array for multibeam base stations," *IEEE Trans. Antennas Propag.*, vol. 68, no. 3, pp. 1378–1388, Mar. 2020.

[11] W. E. I. Liu, Z. N. Chen, and X. Qing, "Broadband low-profile L-prob fed metasurface antenna with TM leaky wave and TE surface wave resonances," *IEEE Trans. Antennas Propag.*, vol. 68, no. 3, pp. 1348–1355, Mar. 2020.

[12] S. Li, Z. N. Chen, T. Li, F. H. Lin, and X. Yin, "Characterization of metasurface lens antenna for sub-6 GHz dual-polarization full-dimension massive MIMO and multibeam systems," *IEEE Trans. Antennas Propag.*, vol. 68, no. 5, pp. 1366–1377, Mar. 2020.

[13] A. H. Abdelrahman, A. Z. Elsherbeni, and F. Yang, "Transmission phase limit of multilayer frequency-selective surface for transmitarray designs," *IEEE Trans. Antennas Propag.*, vol. 62, no. 2, pp. 690–697, Feb. 2014.

[14] H. J. Delgado and M. H. Thursby, "A novel neural network combined with FDTD for the synthesis of a printed dipole antenna," *IEEE Trans. Antennas Propag.*, vol. 53, no. 7, pp. 2231–236, Jul. 2005.

[15] A. A. Minasian and T. S. Bird, "Particle swarm optimization of microstrip antennas for wireless communication systems," *IEEE Trans. Antennas Propag.*, vol. 61, no. 12, pp. 6214–6217, Dec. 2013.

[16] M. F. Pantoja, P. Meincke, and A. R. Bretones, "A hybrid genetic algorithm space-mapping tool for the optimization of antennas," *IEEE Trans. Antennas Propag.*, vol. 55, no. 3, pp. 777–781, Mar. 2007.

[17] P. Robustillo, J. Zapata, J. A. Encinar, and J. Rubio, "ANN characterization of multi-layer reflectarray elements for contoured-beam space antennas in the Ku-band," *IEEE Trans. Antennas Propag.*, vol. 60, no. 7, pp. 3205–3214, Jul. 2012.

[18] P. Robustillo, J. Zapata, J. A. Encinar, and M. Arrebola, "Design of a contoured-beam reflectarray for a EuTELSAT European coverage using a stacked-patch element characterized by an artificial neural network," *IEEE Antennas Wireless. Propag. Lett.*, vol. 11, pp. 977–980, 2012.

[19] G. Gosal, E. Almajali, D. McNamara, and M. Yagoub, "Transmitarray antenna design using forward and inverse neural network modeling," *IEEE Antennas Wireless. Propag. Lett.*, vol. 15, pp. 1483–1486, 2016.

[20] M. Ohira, H. Deguchi, M. Tsuji, and H. Shigesawa, "Multiband single-layer frequency selective surface designed by combination of genetic algorithm and geometry-refinement technique," *IEEE Trans. Antennas Propag.*, vol. 52, no. 11, pp. 2925–2931, Nov. 2004.

[21] H. Choo, A. Hutani, L. C. Trintinalia, and H. Ling, "Shape optimization of broadband microstrip antennas using genetic algorithm," *Electron. Lett.*, vol. 36, no. 25, pp. 2057-2058, 2000.

[22] F. J. Villegas, T. Cwik, Y. Rahmat-Samii, and M. Manteghi, "A parallel electromagnetic genetic-algorithm optimization (EGO) application for patch antenna design," *IEEE Trans. Antennas Propag.*, vol. 52, no. 9, pp. 2424–2435, Sep. 2004.

[23] M. John and M. J. Ammann, "Wideband printed monopole design using a genetic algorithm," *IEEE Antennas Wireless. Propag. Lett.*, vol. 6, pp. 447–449, 2007.

[24] Z. Liu, D. Zhu, S. P. Rodrigues, K.-T. Lee, and W. Cai, "Generative model for the inverse design of metasurfaces," *Nano Lett.*, vol. 18, pp. 6570-6576, 2018.

[25] W. Ma, F. Cheng, Y. Xu, Q. Wen, and Y. Liu, "Probabilistic representation and inverse design of metamaterials based on a deep generative model with semi-supervised learning strategy," *Adv. Mater.*, vol. 31, 1901111, 2019.

[26] R. Zhu, T. Qiu, J. Wang, S. Sui, C. Hao, T. Liu, Y. Li, M. Feng, A. Zhang, C.-W. Qiu, and S. Qu, "Phase-to-pattern inverse design paradigm for fast realization of functional metasurfaces via transfer learning," *Nat. Commun.*, vol. 12, 2974, 2021.

[27] P. Naseri and S. V. Hum, "A generative machine learning-based approach for inverse design of multilayer metasurfaces," *IEEE Trans. Antennas Propag.*, vol. 69, no. 9, pp. 5725-5739, Sep. 2021.

[28] M. Mirza and S. Osindero, "Conditional Generative adversarial nets," 2014, *arXiv: 1411.1784*.

[29] A. Radford, L. Metz, and S. Chintala, "Unsupervised representation learning with deep convolutional generative adversarial networks," 2015, *arXiv: 1511.06434*.

[30] R. J. Langley and A. J. Drinkwater, "Improved empirical model for the Jerusalem cross," *IEEE Proc. H-Microw., Opt. Antennas*, vol. 129, no. 1, pp. 1-6, Feb. 1982.

[31] M. Jiang, Z. N. Chen, Y. Zhang, W. Hong, and X. Xuan, "Metamaterial-based thin planar lens antenna for spatial beamforming and multibeam massive MIMO," *IEEE Trans. Antennas Propag.*, vol. 65, no. 2, pp. 464–472, Feb. 2017.

[32] I. J. Goodfellow, J. Pouget-Abadie, M. Mirza, B. Xu, D. Warde-Farley, S. Ozair, A. Courville, and Y. Bengio, "Generative adversarial nets," 2014, *arXiv: 1406.2661*.

[33] C. G. M. Ryan, M. R. Chaharmir, J. Shaker, J. R. Bray, Y. M. M. Antar, and A. Ittipiboon, "A wideband transmitarray using dual-resonant double square rings," *IEEE Trans. Antennas Propag.*, vol. 58, no. 5, pp. 1486–1493, May. 2010.

[34] A. H. Abdelrahman, P. Nayeri, A. Z. Elsherbeni, and F. Yang, "Bandwidth improvement methods of transmitarray antennas," *IEEE Trans. Antennas Propag.*, vol. 63, no. 7, pp. 2946–2954, Jul. 2015.

[35] G. Liu, H.-J. Wang, J.-S. Jiang, F. Xue, and M. Yi, "A high-efficiency transmitarray antenna using double split ring slot elements," *IEEE Antennas Wireless. Propag. Lett.*, vol. 14, pp. 1415–1418, 2015.

[36] J. Yu, L. Chen, J. Yang, and X. Shi, "Design of a transmitarray using split diagonal cross elements with limited phase range," *IEEE Antennas Wireless. Propag. Lett.*, vol. 15, pp. 1514–1517, 2016.

[37] A. H. Abdelrahman, A. Z. Elsherbeni, and F. Yang, "High-gain and broadband transmitarray antenna using triple-layer spiral dipole elements," *IEEE Antennas Wireless. Propag. Lett.*, vol. 13, pp. 1288–1291, 2014.

[38] C. Xue, Q. Lou, and Z. N. Chen, "Broadband double-layered Huygens's metasurface lens antenna for 5G millimeter-wave systems," *IEEE Trans. Antennas Propag.*, vol. 68, no. 3, pp. 1468–1476, Mar. 2020.

[39] Q. Lou, C. Xue, and Z. N. Chen, "High-efficiency metalens antenna using Huygens's metasurface with glide symmetric I-shape metal strips," *IEEE Trans. Antennas Propag.*, vol. 69, no. 11, pp. .7394-7403, Nov. 2021.

[40] S. So and J. Rho, "Designing nanophotonic structures using conditional deep convolutional generative adversarial networks," *Nanophotonics*, vol. 8, no. 7, pp. 1255-1261, 2019.

[41] T. Qiu, X. Shi, J. Wang, Y. Li, S. Qu, Q. Cheng, T. Cui, and S. Sui, "Deep learning: a rapid and efficient route to automatic metasurface design," *Adv. Sci.*, vol. 6, no. 12, 1900128, 2019.

[42] F. Wen, J. Jiang, and J. A. Fan, "Robust freeform metasurface design based on progressively growing generative networks," *ACS Photonics*, vol. 7, no. 8, pp. 2098-2104, 2020.